Temperature dependence of exciton linewidths in InSb quantum wells

N. Dai, F. Brown, R. E. Doezema, S. J. Chung, and M. B. Santos
Department of Physics and Astronomy and Center for Semiconductor Physics in Nanostructures, The University of Oklahoma, Norman, Oklahoma 73019
(Received 3 August 2000; published 2 March 2001)

We studied the linewidths of excitons in InSb/$Al_{0.09}In_{0.91}Sb$ quantum wells between 4.2 and 300 K using Fourier-transform infrared spectroscopy. Even though the exciton binding energy is only about 1 meV, the absorption is excitonic up to room temperature, due to very weak LO-phonon–electron coupling. The electron-phonon coupling constants and exciton binding energies were obtained through fitting the experimental data. We found that acoustic phonon scattering must be taken into account in fitting the experimental exciton linewidths.

DOI: 10.1103/PhysRevB.63.115321 PACS number(s): 71.35.Cc, 63.20.Kr, 73.21.−b

I. INTRODUCTION

Excitons play a dominant role in the optical properties of semiconductor quantum wells. Their stability, therefore, is important for possible devices exploiting excitons. In low-temperature optical absorption, excitons manifest themselves as sharp peaks. The peaks are broadened with increasing temperature as excitons are scattered and possibly ionized by phonons. At room temperature where electron-phonon scattering is strong, the lifetime of excitons is reduced significantly.

When strong phonon scattering exists, an electron in an exciton state is able to gain enough energy to overcome the capture barrier by absorbing a phonon, leading to breakdown of the electron-hole pair. The thermal capture barrier is proportional to the exciton binding energy, so that excitons having large binding energies tend to be more stable. Thus, a large exciton binding energy is favorable for room-temperature operation of devices based on excitons. In wide-band-gap II-VI semiconductors, the exciton binding energy in the bulk can be as high as 20 meV, which makes it possible to detect excitons even at room temperature. Excitons are less stable in III-V semiconductors such as GaAs, where the exciton binding energy in the bulk is about 5 meV. The binding energy can be enhanced, however, by quantum confinement. In a type-I quantum well, electrons and holes are confined in the same layer, giving rise to a reduction of the exciton Bohr radius and an enhancement of the exciton binding energy. In a perfectly two-dimensional (2D) case (infinitely deep quantum well), the exciton binding energy is 4 times the bulk effective Rydberg. In practical quantum wells, the exciton binding energy is typically about twice the effective Rydberg. In ZnSe/$Zn_{1-x}Mg_xS_ySe_{1-y}$ quantum wells, for instance, the exciton binding energy can be as high as 35 meV (while it is 18 meV in ZnSe bulk). Since the energy of longitudinal optical (LO) phonons in ZnSe is 34 meV, the quantum confinement leads to a significant reduction of LO-phonon–electron coupling that is the dominant scattering mechanism at temperatures above 77 K. The stability of excitons has been studied intensively on wide-band-gap II-VI ZnSe (Ref. 1), $Zn_{1-x}Cd_xSe$ (Ref. 2), $Cd_xZn_{1-x}Te$ (Ref. 3), and CdTe (Refs. 4 and 5) quantum wells. There are also some reported studies on III-V GaAs (Refs. 6 and 7) and $In_xGa_{1-x}As$ (Refs. 8 and 9) quantum wells. Room-temperature excitons have been reported on many II-VI and III-V quantum wells.[3,7] Among them, a $In_xGa_{1-x}As/In_xAl_{1-x}As$ quantum well had the narrowest band gap (773 meV in $In_xGa_{1-x}As$).

InSb-based quantum wells are potentially useful for the fabrication of devices such as light-emitting diodes and laser diodes in the mid-infrared region. In bulk InSb, excitons have a binding energy of only 0.5 meV and a very large Bohr radius of 600 Å. Although exciton transitions have been observed at liquid-helium temperature in extremely pure InSb bulk,[10,11] one expects exciton ionization above the temperature where LO-phonon scattering starts to take effect. However, we find that in InSb-based quantum wells, excitons are observable in optical absorption spectra up to room temperature. Previous work reported exciton spectra in square[12] and parabolic[13] quantum wells at low temperatures. Here we report the observation of room-temperature excitons in InSb/$Al_{0.09}In_{0.91}Sb$ quantum wells and the investigation of the exciton linewidth broadening due to impurities and acoustic-phonon and LO-phonon scattering. The observation of room-temperature excitons suggests also that InSb can be used to fabricate room-temperature exciton-based devices.

II. SAMPLE GROWTH AND PREPARATION

Our InSb/$Al_{0.09}In_{0.91}Sb$ quantum wells were grown by molecular beam epitaxy on semi-insulating (001) GaAs substrates.[14] The samples were nominally undoped with a background density of ionized impurities on the order of $10^{15}\,cm^{-3}$.[15,16] In order to isolate dislocations due to large lattice mismatch between the substrate and the epilayer, a thick buffer layer was grown prior to the growth of the quantum-well structure. The buffer consists of an $Al_{0.09}In_{0.91}Sb$/InSb superlattice sandwiched between two 2-μm $Al_{0.09}In_{0.91}Sb$ layers. The barrier layers, with nominally 9% Al concentration, are unstrained and the strained InSb well layers are thin enough to be pseudomorphic, as confirmed by x-ray diffraction measurements, which showed the excellent crystal quality of the samples. The three samples discussed here have the same barrier thickness of 500 Å and different well thickness $L_w = 225$, 250, and 275 Å. There are a total of 25 quantum wells in each of these

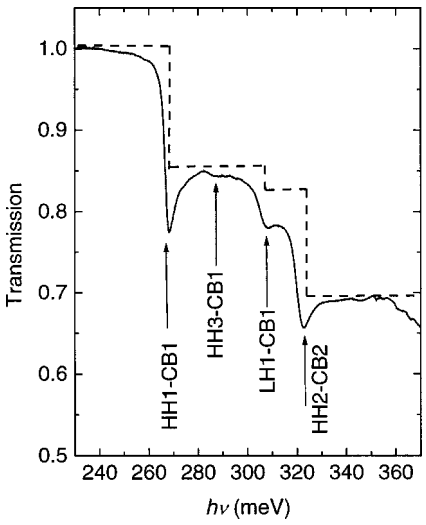

FIG. 1. Optical absorption spectrum (plotted as transmission vs. photon energy) measured on the 225-Å quantum wells at 4.2 K. The spectrum shows a number of excitonic transitions, labeled by HH1-CB1, HH2-CB2, LH1-CB1, HH3-CB1 in the figure, riding on the steplike 2D continuum sketched by the dashed line.

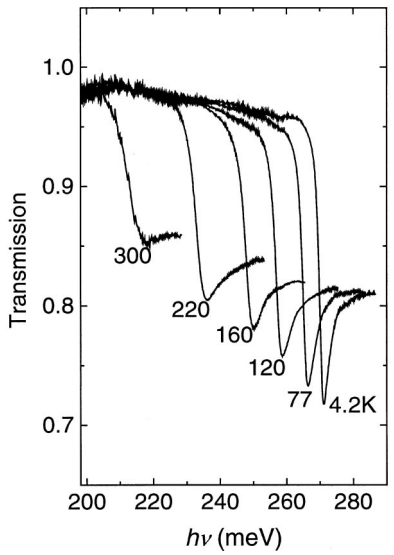

FIG. 2. Absorption spectra (plotted as transmission vs photon energy) in the HH1-CB1 transition region at 4.2, 77, 120, 160, 220, and 300 K for 225-Å quantum wells.

samples. The growth surfaces of the samples were coated with NiCr layers by thermal evaporation in order to suppress Fabry-Perot interference.[17] We use a Bio-Rad 60-Å Fourier-transform infrared (FTIR) spectrometer equipped with a variable-temperature Dewar to probe the interband excitonic transitions. The temperature of the sample can be controlled from 4.2 K to room temperature.

III. EXPERIMENTAL RESULTS AND DISCUSSION

A. Excitons at room temperature

Figure 1 shows an optical absorption spectrum measured on the sample with $L_w = 225$ Å at 4.2 K. The main features of the spectrum are well-defined exciton lines riding on the steplike 2D exciton continuum. These lines are not separated from the continuum since the binding energy of the excitons in our system is, even including the quantum confinement effect, about 1 meV. We use HH, LH, and CB to represent heavy-hole, light-hole, and conduction-band energy states, respectively, and n denotes the subband index. Thus, the transition from the heavy-hole ground state to the conduction-band ground state is designated by HH1-CB1. As shown in the figure, excitons associated with the HH1-CB1, LH1-CB1, and HH2-CB2 transitions as well as the ''forbidden'' HH3-CB1 transition are clearly observed. The assignment of the transition peaks is based on comparison with a four-band model calculation[13] described by Bastard.[18] Due to the strain in the system and the different effective masses of heavy holes and light holes ($0.27m_0$ and $0.014m_0$, respectively), the LH1-CB1 transition is well above the HH1-CB1 transition in energy. The forbidden HH3-CB1 transition is near the HH1-CB1 peak but is quite weak. Thus, the line shape of the HH1-CB1 transition is essentially unaffected by other excitonic transitions. We therefore choose the HH1-CB1 exciton line for the focus of our study.

Figure 2 presents the HH1-CB1 excitonic transition measured on the $L_w = 225$ Å sample at temperatures between 4.2 K and room temperature. As the temperature is increased, the exciton line becomes broader but is still clearly visible up to room temperature. To our knowledge, the InSb quantum well is the system with the narrowest band gap for which room-temperature excitons are observed. Since the exciton lines overlap with the exciton continuum (see Figs. 1 and 2), we have to rely on modeling to separate these two parts in order to extract useful information from these spectra. Both Gaussian and Lorentzian line shapes have been used to fit exciton lines. Young *et al.*[19] argued that a Lorentzian line should be used when the broadening is dominated by homogeneous scattering and a Gaussian line shape for inhomogeneous scattering. In reality, an exciton line is neither pure Gaussian nor pure Lorentzian, because an experimental exciton line is not symmetric with respect to the center of the peak. Since we are interested only in the variation of the exciton linewidth with temperature and not in the absolute values, we expect that fitting the experimental curves with either a Gaussian or a Lorentzian oscillator will give similar results. In our case, we find that the exciton line is better reproduced by a Lorentzian oscillator than by a Gaussian one, implying weak inhomogeneous scattering in our system. Since other transitions make a negligible contribution to the line shape in the HH1-CB1 region, we model the experimental HH1-CB1 absorption spectrum (exciton+continuum) by

$$\Theta(E) = \alpha - S(E_c - E)\frac{I_c}{1+\exp[(E_c-E)/\Gamma_c]} - \frac{2}{\pi}\frac{I_e\Gamma_e}{4(E-E_e)^2+\Gamma_e^2}, \quad (1)$$

where $S(E_c-E)$ is the Sommerfeld factor:[20]

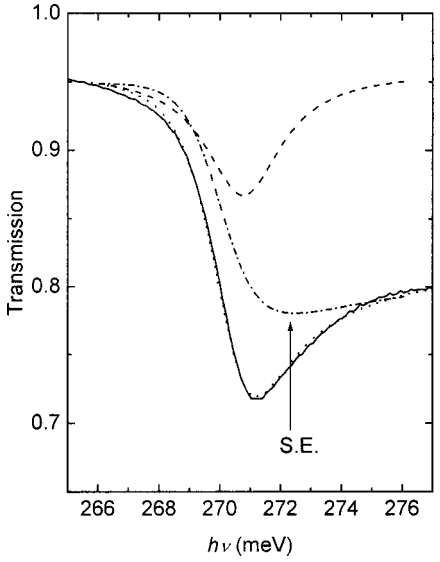

FIG. 3. A 4.2-K experimental HH1-CB1 spectrum (the solid line) and a theoretical fit (the dotted line) calculated using Eq. (1) for the 225-Å quantum-well sample. The corresponding Lorentzian oscillator (dashed line) and the calculated continuum (dot-dashed line) are also shown. The weak valley on the calculated continuum is due to the Sommerfeld enhancement (arrow).

$$S(E_c-E)=\begin{cases} 2 & E\leqslant E_c \\ \dfrac{2}{1+\exp[-2\pi\sqrt{R/(E-E_c)}]}, & E>E_c \end{cases}$$

In Eq. (1) and the expression above, the first term, α, is a constant, defining the transmission of the overall spectrum. The second term represents exciton continuum absorption modified by a Sommerfeld enhancement factor, with Γ_c being the broadening parameter of the continuum, R being the exciton effective Rydberg, and I_c corresponding to the step height of the 2D continuum. The third term is a Lorentzian oscillator used to describe exciton absorption, with Γ_e being the broadening parameter and I_e the integrated peak intensity of the exciton line. E_c and E_e are the energy positions of the continuum and the exciton peak, respectively. The calculation using Eq. (1) reproduces a spectrum in excellent agreement with the experimental spectrum, as shown by the thick solid curve (experimental) and the dotted one (theoretical) in Fig. 3. The Lorentzian oscillator and the continuum contributions are depicted separately in the figure. As marked in the figure, the Sommerfeld correction to the exciton continuum causes a weak absorption maximum peak at energies above the exciton continuum. Although there are a total of seven fitting parameters in Eq. (1), we find that their contributions to the line shape are mutually independent in the fitting process. Using Eq. (1) to fit the experimental absorption spectra in the wavelength range of the HH1-CB1 transition, we obtained broadening parameters, integrated peak intensities (or step height for the exciton continuum), and peak positions for both the exciton and the continuum transitions.

The exciton binding energy, E_c-E_e, can be obtained through fitting using Eq. (1). Due to the 2D confinement in the quantum wells, the exciton binding energy is expected to be larger than 0.5 meV (exciton binding energy in the bulk). Through fitting the experimental data at temperatures below 77 K for all three samples, we obtain reasonable exciton binding energies in the range between 0.6 and 1 meV, but we are unable to resolve differences between binding energies of the different samples. As temperature increases, however, it becomes increasingly difficult to determine the binding energy for such weak excitons due to the increasing peak broadening and the mixing with the absorption maximum due to the Sommerfeld enhancement (see Fig. 3).

Fitting the experimental spectra using Eq. (1) shows that the spectra are excitonic up to room temperature. At first glance, exciton observation at room temperature is surprising in a system in which the exciton binding energy is so much smaller than the LO-phonon energy (at room temperature, I_e obtained from fitting the experimental curves is around 50% of that at 4.2 K). Electron-hole pairs can be easily broken with increasing temperature as the number of phonons increases. Two factors make it possible to understand our observation.

The first is our experimental technique. Typically, excitons are studied using optical absorption or photoluminescence techniques. In a photoluminescence measurement, electrons are photopumped into energy levels above the bottom of the conduction band, becoming hot electrons. The hot electrons then relax to the bottom of the conduction band by emitting phonons and/or exchanging energies with defects and dislocations. If the electrons in the conduction band recombine with holes in the valence band, they only contribute to continuum emission. The observation of exciton emission requires that the electrons in the bottom of the conduction band further relax to exciton states and then recombine with holes. At low temperature, the recombination occurs quickly at a time constant $\approx$500 ps in GaAs/$Al_xGa_{1-x}As$,[21] for instance. However, this recombination rate decreases with increasing temperature as the rate of phonon ionization of excitons increases. Thus, excitonic photoluminescence can be suppressed at high temperature, as shown in many reports. In optical absorption, however, an exciton is formed by photon absorption, leaving a signature on the absorption spectrum. The energy of the photon absorbed by the electron has an uncertainty corresponding to the final-state exciton linewidth. Thus, excitonic absorption can take place even at high temperature. Furthermore, photoluminescence becomes less useful for materials in which the luminescence efficiency is significantly decreased. Optical absorption, on the other hand, essentially maps the density of states so that it is not sensitive to defects that have a much lower density of states.

The second factor needed to understand our observations is the weak LO-phonon–electron coupling in our systems, as will be discussed in the following section. The weak coupling makes it easy for the exciton signature to be resolved after a careful line-shape analysis to separate the exciton line from the background and the continuum absorption. Our study shows that optical absorption is a highly suitable technique for the detection of excitons in semiconductor materials in which excitons are weakly bound.

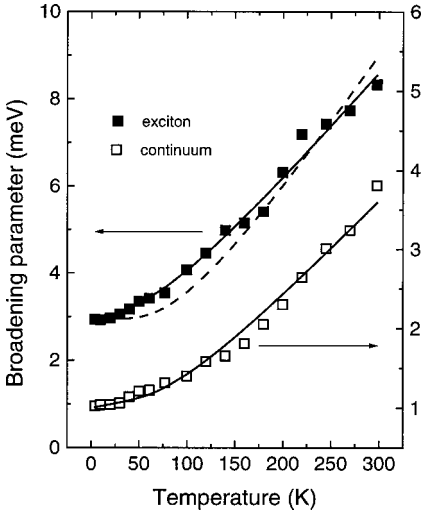

FIG. 4. Experimental exciton and continuum linewidths as a function of temperature measured on $L_w = 275$ Å quantum wells. The solid curves are the fit to the experimental data using Eq. (2) and the dashed curve is the fit to the exciton linewidth by ignoring scattering by acoustic phonons.

B. Exciton linewidth

Experimental HH1-CB1 exciton and continuum linewidths as a function of temperature are presented in Fig. 4 for the 225-Å quantum wells. The linewidths of the exciton and the continuum have a similar temperature dependence. However, the broadening parameter of the excitons is nearly 3 times that of the continuum at low temperatures. In fact, one should not compare the two linewidths directly, since the 2D effect modifies the density of states of the free electrons and the density of states of the excitons in quite different ways. The 3D density of states of the form of $\sim(E-E_0)^{1/2}$ (continuum) becomes steplike due to 2D confinement, while the density of states of the exciton is not significantly changed from 3D to 2D since excitons are localized states.[18] As a result, the 2D effect modifies the linewidth of electrons in the continuum significantly, but only weakly affects the linewidth of the excitons. We measured the continuum absorption of a high quality 3-μm InSb epilayer grown on a GaAs substrate in the same growth condition, finding that the linewidth was in fact about 5% larger than that of the HH1-CB1 exciton.

In semiconductors, the temperature-independent inhomogeneous broadening is due to the scattering from ionized impurities, point and dislocation defects, alloy fluctuation, and interfacial roughness. The temperature-dependent homogeneous broadening is due to scattering by phonons. (Electron scattering[22] is negligible here). The temperature dependence of the exciton linewidth (or the continuum) can be described by[23]

$$\Gamma(T)=\Gamma_I+\gamma_A T+\frac{\Gamma_{\mathrm{LO}}}{\exp(\hbar\omega_{\mathrm{LO}}/k_B T)-1}, \tag{2}$$

where ω_{LO} is the LO-phonon frequency, Γ_I is inhomogeneous broadening, γ_A accounts for broadening due to acoustic phonon scattering, and Γ_{LO} is due to the scattering by LO phonons. At low temperature (typically below 100 K) where the effect of LO-phonon scattering is not significant, Γ_I is the dominant factor for the overall spectral broadening. We fit the experimental Γ as a function of temperature using Eq. (2) and the results are presented in Fig. 4 by the solid curves. Parameters Γ_I, γ_A, and Γ_{LO} obtained through fitting are listed in Table I.

We are able to grow materials with very high quality, as demonstrated by the distinct exciton lines in Figs. 1 and 2. We expect a very low density of defects and dislocations since the samples are unrelaxed, as confirmed by x-ray diffraction measurements. Furthermore, the compositional fluctuation is negligible since the excitons in our samples are localized in InSb wells. Thus, we expect that the dominant contributions to Γ_I come from two parts: the interfacial roughness and ionized impurities. Due to the use of the relatively large well widths in our samples, the effect of interface roughness is small. Interface roughness may become an overwhelming contribution to inhomogeneous broadening for narrow quantum wells.[24,25] The interfacial roughness can be estimated as a one-monolayer ($\sim$3-Å) fluctuation in well thickness, corresponding to about 1-meV uncertainty in the energy of the HH1-CB1 transition in the samples discussed here.

The contribution to Γ_I by ionized impurities is due to the Stark effect in a random Coulomb field, which takes the form of[10]

$$\Delta E_s \approx 2\times 10^{-30} N_i^{4/3}\left(\frac{m_0}{\mu}\right)^2 E_b^{-1} \tag{3}$$

for spherically symmetric states. In Eq. (3), μ and E_b are the reduced effective mass and the binding energy of the exciton, respectively; N_i is the density of ionized impurities and m_0 the mass of a bare electron. From our previous studies on samples grown with the same growth parameters,[15,16] it is

TABLE I. Inhomogeneous broadening Γ_I at 4.2 K as well as acoustic-phonon–electron coupling constant γ_A and LO-phonon–electron coupling Γ_{LO} obtained through fitting the experimental data for samples with well width $L_W = 225$, 250, and 275 Å using Eq. (2) with $R = 0.5$. The numbers in parentheses are obtained from fitting the continuum lines.

L_W (Å)	Γ_I (meV)	γ_A (μeV/K)	Γ_{LO} (meV)
225	2.8±0.5 (1.2±0.2)	9.6±1.4 (3.5±0.7)	4.4±0.8 (1.6±0.4)
250	3.4±0.6 (1.2±0.2)	11.3±1.8 (5.2±0.8)	4.0±1.0 (1.2±0.4)
275	2.8±0.5 (1.0±0.2)	9.6±1.1 (2.3±0.5)	4.4±0.6 (2.9±0.6)

expected that N_i is the order of $10^{15}\,\mathrm{cm}^{-3}$ in our samples. Using Eq. (3), we estimate that the broadening contributed by ionized impurities is roughly 1 meV (using $\mu \sim 0.014 m_0$ and $E_b \sim 1$ meV). We expect therefore that ionized impurity scattering and interfacial roughness make roughly equal contributions to the listed experimental values of Γ_I in Table I.

In semiconductors, γ_A is typically on the order of several μeV/K, while Γ_{LO} ranges in values from a few to several hundred meV depending on the strength of LO-phonon–electron coupling. The strong LO-phonon–electron coupling comes about when the long-wavelength LO phonon gives rise to an electric field that interacts with a highly polarized exciton. Sometimes this kind of coupling can be strong enough to break the electron-hole pair. Indeed, γ_A was ignored in most cases in fitting experimental $\Gamma(T)$ because excitons in II-VI materials are so strongly polarizable that the interaction with LO phonons dominates. However, the destabilization of excitons due to strong LO-phonon–exciton coupling is balanced by the large exciton binding energies in these materials. As a result, signatures of room-temperature excitons are observed in a number of II-VI semiconductors. For GaAs systems with a band gap of 1.42 eV and exciton binding energy around 12 meV (5 meV in bulk), Γ_{LO} is ~ 6 meV, only $\frac{1}{30}$ of that of ZnSe. In spite of the smaller exciton binding energy in $\mathrm{GaAs/Al}_x\mathrm{Ga}_{1-x}\mathrm{As}$ quantum wells, room-temperature excitons have been observed owing to the relatively weak LO-phonon–exciton coupling. Note that the quantum confinement only changes the exciton binding energy, not the electron-phonon coupling.[21]

Assuming a Fröhlich type of interaction, the coupling constant Γ_{LO} can be expressed by[26,3]

$$\Gamma_{\mathrm{LO}} \propto \alpha_F \hbar \omega_{\mathrm{LO}} \left(1 + \frac{m_e}{m_h}\right)^{1/2}, \tag{4}$$

where α_F is the Fröhlich electron-phonon interaction constant, which can be written as[26]

$$\alpha_F = e^2 [\epsilon_\infty^{-1} - \epsilon_0^{-1}] \left(\frac{m_e}{2\hbar^3 \omega_{\mathrm{LO}}}\right)^{1/2}. \tag{5}$$

In Eqs. (4) and (5), ϵ_∞, ϵ_0, m_e, and m_h are the optical dielectric constant, the static dielectric constant, the electron effective mass, and the hole effective mass, respectively. Using Eqs. (4) and (5), one obtains $\Gamma_{\mathrm{LO}}(\mathrm{InSb})/\Gamma_{\mathrm{LO}}(\mathrm{GaAs}) \sim 0.25$. Fitting the experimental data in Fig. 4 gives $\Gamma_{\mathrm{LO}} \sim 4$ meV, to be compared to 6 meV in GaAs.[27] Since Γ_{LO} is small in our systems, the contribution to the exciton linewidth by acoustic phonons can no longer be ignored. This is demonstrated by the dashed lines in Fig. 4 showing the fit to the experimental data by ignoring the acoustic-phonon–electron coupling. As can be calculated using Eq. (2) and the numbers in Table I, the second term in Eq. (2) is even larger than the third term below 77 K. Thus, in our system the need to include the acoustic phonon is not due to especially strong acoustic-phonon–electron coupling but due to relatively weak LO-phonon–electron coupling.

Clearly, at high temperature the stability of an exciton relies on the competition between the exciton binding energy and the strength of the LO-phonon–electron coupling, not only on the binding energy. In our system, the relatively small Γ_{LO} permits the observation of room-temperature excitons.

IV. SUMMARY

We have measured the strengths and linewidths of excitonic absorption in $\mathrm{InSb/Al}_{0.09}\mathrm{In}_{0.91}\mathrm{Sb}$ quantum wells from 4.2 K to room temperature. Although the excitons in the system are very weakly bound, the absorption spectra are excitonic up to room temperature. The observation of room-temperature excitons is due to the use of the absorption technique and due to the weak LO-phonon–electron coupling in the quantum wells. Also because of the weak LO-phonon–electron coupling, scattering by acoustic phonons has to be taken into account in fitting the experimental linewidth as a function of temperature.

ACKNOWLEDGMENTS

This work was supported by NSF Grants Nos. DMR-9973167 and EPS-9720651.

[1] Yoichi Yamada and Tsunemasa Taguchi, J. Cryst. Growth **101**, 661 (1990).
[2] I. J. Blewett, D. J. Bain, A. Tookey, G. Brown, I. Galbraith, A. K. Kar, B. Vögele, K. A. Prior, B. C. Cavenett, and B. S. Wherrett, Phys. Rev. B **59**, 9756 (1999).
[3] D. Lee, A. M. Johnson, J. E. Zucker, R. D. Feldman, and R. F. Austin, J. Appl. Phys. **69**, 6722 (1991).
[4] M. O'Neill, M. Oestreich, and W. W. Röhle, Phys. Rev. B **48**, 8980 (1993).
[5] R. Hellmann, M. Koch, J. Feldman, S. T. Cundiff, E. O. Göbel, D. R. Yakovlev, A. Waag, and G. Landwehr, Phys. Rev. B **48**, 2847 (1993).
[6] J. Lee, E. S. Koteles, and M. O. Vassell, Phys. Rev. B **33**, 5512 (1986).
[7] J. Filipowicz, C. Ghezzi, and L. Tarricone, Solid State Commun. **74**, 533 (1990).
[8] C. Arena, B. Rotelli, and L. Tarricone, Phys. Status Solidi B **185**, 505 (1994).
[9] Orani, A. Polimeni, A. Patanè, M. Capizzi, F. Martelli, A. D'Andrea, N. Tomassini, P. Borri, M. Gurioli, and M. Colocci, Phys. Status Solidi A **164**, 107 (1997).
[10] L. M. Kanskaya, S. I. Kokhanovskii, and R. P. Seisyan, Fiz. Tekh. Poluprovodn. **13**, 2424 (1979) [Sov. Phys. Semicond. **13**, 1420 (1979)].
[11] V. I. Ivanov-Omskii, S. I. Kokhanovskii, R. P. Seisyan, V. A. Smirnov, and Sh. U. Yuldashev, Fiz. Tekh. Poluprovodn. **17**, 532 (1983) [Sov. Phys. Semicond. **17**, 334 (983)].
[12] N. Dai, F. Brown, P. Barsic, G. A. Khodaparast, R. E. Doezema, M. B. Johnson, S. J. Chung, K. J. Goldammer, and M. B. Santos, Appl. Phys. Lett. **73**, 1101 (1998).

[13] N. Dai, G. A. Khodaparast, F. Brown, R. E. Doezema, S. J. Chung, and M. B. Santos, Appl. Phys. Lett. **76**, 3905 (2000).
[14] S. J. Chung, M. A. Ball, S. C. Lindstrom, M. B. Johnson, and M. B. Santos, J. Vac. Sci. Technol. B **18**, 1583 (2000).
[15] S. J. Chung, K. J. Goldammer, S. C. Lindstrom, M. B. Johnson, and M. B. Santos, J. Vac. Sci. Technol. B **17**, 1151 (1999).
[16] K. J. Goldammer, W. K. Liu, G. A. Khodaparast, S. C. Lindstrom, M. B. Johnson, R. E. Doezema, and M. B. Santos, J. Vac. Sci. Technol. B **16**, 1367 (1998).
[17] S. W. McKnight, K. P. Stewart, H. D. Drew, and K. Moorjani, Infrared Phys. **27**, 327 (1987).
[18] G. Bastard, *Wave Mechanics Applied to Semiconductor Heterostructures* (Les Editions Physique, Les Ulis, 1988).
[19] P. M. Young, E. Runge, M. Ziegler, and H. Ehrenreich, Phys. Rev. B **49**, 7424 (1994).
[20] Masaki Shinada and Satoru Sugano, J. Phys. Soc. Jpn. **21**, 1936 (1966).
[21] J. Feldmann, J. Nunnenkamp, G. Peter, E. Göbel, P. Dawson, K. J. Moore, C. T. Foxon, and R. J. Elliot, Phys. Rev. Lett. **59**, 2337 (1987).
[22] Wei Liu, Desheng Jiang, Kejian Luo, Yaohui Zhang, and Xiaoping Yang, Appl. Phys. Lett. **67**, 679 (1995).
[23] A. J. Fisher, W. Shan, J. J. Song, Y. C. Chang, R. Horning, and B. Goldenberg, Appl. Phys. Lett. **71**, 1981 (1997); D. S. Kim, J. Shah, J. E. Cunningham, T. C. Damen, W. Schäfer, M. Hartmann, and S. Schmitt-Rink, Phys. Rev. Lett. **68**, 1006 (1992).
[24] C. Weisbuch, R. Dingle, A. C. Gossard, and W. Wiegmann, Solid State Commun. **21**, 133 (1977).
[25] D. F. Welch, G. W. Wicks, and L. F. Eastman, Appl. Phys. Lett. **46**, 991 (1985).
[26] H. Fröhlich, Adv. Phys. **3**, 325 (1954).
[27] D. A. B. Miller, D. S. Chemla, D. J. Eilenberger, P. W. Smith, A. C. Gossard, and W. T. Tsang, Appl. Phys. Lett. **41**, 679 (1982).